Electronic structure, bonding and phonon modes in the negative thermal expansion materials of $Cd(CN)_2$ and $Zn(CN)_2$

2008 J. Phys.: Condens. Matter 20 275224

(http://iopscience.iop.org/0953-8984/20/27/275224)

J. Phys.: Condens. Matter **20** (2008) 275224 (8pp) doi:10.1088/0953-8984/20/27/275224

Electronic structure, bonding and phonon modes in the negative thermal expansion materials of $Cd(CN)_2$ and $Zn(CN)_2$

Pei Ding[1,2], E J Liang[1,3], Yu Jia[1] and Z Y Du[1]

[1] School of Physics and Engineering, Zhengzhou University, Zhengzhou 450052, People's Republic of China
[2] Department of Mathematics and Physics, Zhengzhou Institute of Aeronautical Industry Management, Zhengzhou 450015, People's Republic of China

E-mail: ejliang@zzu.edu.cn

Received 20 December 2007, in final form 19 May 2008
Published 4 June 2008
Online at stacks.iop.org/JPhysCM/20/275224

Abstract

The disordered configuration, band structures, density of states, Mulliken population, elastic constants, zone center optic phonon modes and their Grüneisen parameters of $M(CN)_2$ (M = Cd, Zn) have been studied for possible cyanide-ordering patterns by the first-principles plane-wave pseudopotential method based on density functional theory. Total energy calculations predict that MC_2N_2–MC_2N_2 is the most favorable configuration for $Cd(CN)_2$ whereas all three possible configurations are near equally favorable for $Zn(CN)_2$. Effective charges and bond order analyses reveal that the $M(CN)_2$ (M = Cd, Zn) frameworks include much stiffer C≡N and weaker M–C/N bonds, which account for the flexing of the M–CN–M linkage during the transverse motion of the cyanide-bridge. The transverse translational and the librational modes give rise to negative Grüneisen parameters and therefore contribute to the negative thermal expansion. Transverse vibrations of the C and N atoms in the same (transverse translational modes) or opposite (librational modes) directions have the same effect of drawing the anchoring metal atoms closer. Among all the optical phonon modes, the lowest-energy transverse translational optical modes which are neither Raman nor infrared active in $Cd(CN)_2$ and $Zn(CN)_2$ give rise to the largest contribution to the negative thermal expansion.

(Some figures in this article are in colour only in the electronic version)

1. Introduction

Materials with negative thermal expansion (NTE) have received considerable attention due to scientific curiosity and technological interest. Increasing families of such materials such as AM_2O_8 (A = Zr, Hf; M = W, Mo) [1–3], AM_2O_7 (A = Zr; M = V, P) [4], AM_3O_{12} (A = Sc, Y, etc; M = W, Mo) [5], AO_2 (zeolites, $AlPO_4$-17) [6, 7], AMO_5 ($NbOPO_4$) [8, 9] and A_2O (Cu_2O, Ag_2O) [10, 11] have been reported. Recently, $M(CN)_2$ (M = Cd, Zn) [12–14] and Prussian blue families [15–17] were found to have strong NTE. Among these families, $Cd(CN)_2$ and $Zn(CN)_2$ were found to have largest and isotropic NTE coefficients which are respectively -20.4×10^{-6} K^{-1} from 150 to 375 K and -16.9×10^{-6} K^{-1} from 25 to 375 K [13], approximately twice as large as that of ZrW_2O_8 [1]. Their structure can be regarded as a framework of metal–cyanide–metal (M–CN–M′) polyhedra. Each metal center binds four cyanide ligands in a tetrahedral arrangement and each ligand acts as a linear bridge between two metal centers. There have been conflicting reports on the degree of cyanide ordering in the $M(CN)_2$ framework structure with fully ordered in which MC_4 and MN_4 tetrahedra alternate [18], or fully disordered in which MC_xN_{4-x} tetrahedra are interlinked due to the C–N orientational disorder [12, 19]. The space group determined from single crystal x-ray diffraction analysis was $P\bar{4}3m$ (fully ordered) and exchanging C and N atoms did not significantly alter the refinement parameters [18]. A neutron diffraction study [12] found that a disordered structure with space group

[3] Author to whom any correspondence should be addressed.

$Pn\bar{3}m$ [20] fitted equally well to the diffraction pattern. Although further studies by x-ray diffraction [13, 14] and Raman and infrared spectroscopy [21] supported statistical C–N orientational disorder in both $Cd(CN)_2$ and $Zn(CN)_2$, the origin for the possible ordered or disordered structures remains unclear and needs to be clarified.

Goodwin *et al* [13] analyzed the intrinsic geometric flexibility of framework structures of $Zn_xCd_{1-x}(CN)_2$ using a reciprocal-space dynamical matrix approach and suggested that a large number of low energy rigid unit modes (RUMs) gave rise to the extraordinarily large NTE behavior, regarding ZnC_xN_{4-x} tetrahedra as rigid units based on the assumption that M–C/N bonding possesses significant covalent character. Chapman *et al* [14] probed the instantaneous structure of $Zn(CN)_2$ using atomic pair distribution function analysis of high energy x-ray scattering data (100–400 K) and suggested that the population of transverse vibrational modes of the bridging atoms was the mechanism underlying the NTE. Dispersionless rigid unit modes at about 2 meV ($\sim$16 cm^{-1}) were also observed by time of flight inelastic neutron scattering from powdered samples of $Zn(CN)_2$ [22]. The Raman and infrared spectroscopic study in $Zn(CN)_2$ gave the lowest optical phonon mode at 178 cm^{-1} ($\sim$22 meV) [21]. Therefore, a systematic study on the geometric and electronic structure, bonding character and phonon modes of these materials is necessary for understanding their NTE mechanisms.

In this paper, we present a systematic study on the $M(CN)_2$ structures with cyanide-bridges, aimed at the above mentioned problems using the first-principles plane-wave pseudopotential method based on density functional theory [23]. Besides the possible ordered or disordered structures from minimum energy calculations, the electronic structure, bond character and atomic vibrations are studied with an attempt to understand the super-NTE behavior of these materials.

2. Method of calculation

The first-principles calculations on electronic structure, bonding and elastic constants were performed using the CASTEP code [24] with ultrasoft pseudopotential plane-wave basis sets. The exchange and correlation (XC) energy of the electrons was described by GGA of PBE [25] and LDA of CA-PZ [26]. Ultrasoft Vanderbilt-type pseudopotentials [27] with electronic configurations of Cd $4d^{10}5s^2$, Zn $3d^{10}$ $4s^2$, C $2s^2$ $2p^2$ and N $2s^2$ $2p^3$ were used. The maximum plane-wave cutoff energy was taken as 600 eV and the numerical integration of the Brillouin zone was performed by using a $4 \times 4 \times 4$ Monkhorst–Pack k-point sampling [28]. As far as the symmetry of the crystals investigated was concerned, the numbers of k-point was not large. However it was sufficient here as both materials investigated turn out to be insulators and the k-point meshes to $6 \times 6 \times 6$ changed the total energy by less than 0.01 eV/atom. The cutoff energy and k-point sampling parameters were tested for convergence. The tolerance of 5×10^{-7} eV/atom was adopted for the self-consistent calculations to control the electronic minimization algorithm. Geometry energetic minimization was accomplished by using convergence thresholds of 5×10^{-6} eV/atom for total energy, 0.01 eV $Å^{-1}$ for maximum force, 0.02 GPa for pressure and 5×10^{-4} Å for displacement. Geometry optimization was performed without symmetry constraints. The minimum total energy of each structure was achieved by automatically relaxing the lattice parameters and atomic positions using the Broyden–Fletcher–Goldfarb–Shanno (BFGS) algorithm [29]. A Monkhorst–Pack mesh of $8 \times 8 \times 8$ special k-points sampling was chosen while the partial density of states (PDOS) was calculated. Mulliken overlap populations [30] were performed by using a projection of the plane-wave electronic states onto a localized linear combination of atomic orbitals (LCAO) basis set and integrated with a distance cutoff of 3 Å. The convergence thresholds of 1.0×10^{-6} eV/atom, 0.002 eV $Å^{-1}$ and 1.0×10^{-4} Å for energy change, maximum force and maximum displacement were used for the elastic constants calculation.

The zone center phonon modes and phonon DOS were also calculated using CASTEP but with the norm-conserving pseudopotentials [31] and the local density approximation (LDA of CA-PZ). The maximum plane-wave cutoff energy and the k-points sampling were set as 900 eV and $4 \times 4 \times 4$, respectively. First, the geometry optimization relaxing both the lattice parameters and the atomic positions were performed with the same convergence tolerance mentioned above. Next, the vibrational properties were calculated using the linear response methodology [32] with the convergence criterion of 1×10^{-5} eV/atom for the electronic eigenvalues. The zone center phonon frequencies obtained under different hydrostatic pressures (from 0 to 1.0 GP with increment of 0.2 GP) were used to calculate the Grüneisen parameters of the phonon modes for $Cd(CN)_2$ and $Zn(CN)_2$. A $4 \times 4 \times 4$ Monkhorst–Pack grid was used which corresponded to an actual spacing of 0.04 $Å^{-1}$ while the phonon density of states of $Zn(CN)_2$ was calculated. The integration method interpolating the eigenvalues from the CASTEP calculation onto a finer k-point grid of about $200 \times 200 \times 200$ was applied while the phonon DOS was represented (see figure 5).

3. Results and discussion

In the following paragraphs, the systematic investigation of geometric and electronic structure, bonding character and atomic vibrations (phonon modes) for the $M(CN)_2$ framework based on the first-principles calculations are presented. The NTE mechanisms are discussed based on our bonding character and phonon mode analyses.

3.1. Crystal structures

Considering all possible MC_xN_{4-x} tetrahedron geometries in the crystal, three unit cells were proposed here for the local minimum configuration of the $M(CN)_2$ (M = Cd, Zn) crystal. Figures 1(a)–(c) show the unit cells with cyanide-bridged MC_4 and MN_4 tetrahedra, with MC_3N and MCN_3 tetrahedra and with two MC_2N_2 tetrahedra, respectively. The results for the equilibrium lattice parameters, cell volumes, total energy of the three possible atomic arrangements of $Cd(CN)_2$ and

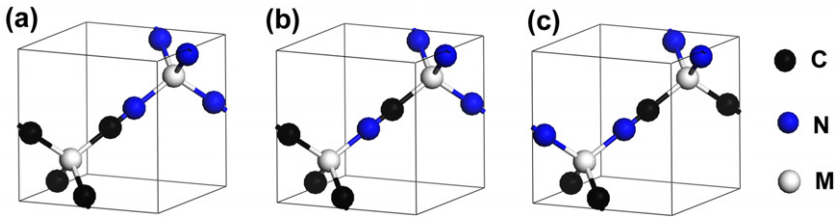

Figure 1. Ball-and-stick models of $M(CN)_2$ (M = Cd, Zn) for (a) MC_4–MN_4, (b) MCN_3–MC_3N, and (c) MC_2N_2–MC_2N_2 tetrahedra geometries.

Table 1. Crystal structure and electronic properties of $Cd(CN)_2$. 'M4', 'M13' and 'M22' represent the tetrahedra configuration of CdC_4–CdN_4, $CdCN_3$–CdC_3N and CdC_2N_2–CdC_2N_2, respectively.

	LDA–CA-PZ			GGA–PBE			
Model	M4	M13	M22	M4	M13	M22	Exp. [13]
a (Å)	6.3163	6.3147	6.3969	6.4928	6.49158	6.5466	6.3249
b (Å)	6.3163	6.3147	6.3969	6.4928	6.49128	6.5469	6.3249
c (Å)	6.3162	6.3147	6.1433	6.4928	6.49138	6.3748	6.3249
Cell volume ($Å^3$)	251.99	251.80	251.38	273.71	273.53	273.22	253.02
Energy/unit cell (eV)	−4271.354	−4271.391	−4271.404	−4268.038	−4268.087	−4268.103	
Band gap (eV)	5.85	5.78	5.73	6.00	5.93	5.91	

Table 2. Crystal structure and electronic properties of $Zn(CN)_2$. 'M4', 'M13' and 'M22' represent the tetrahedra configuration of ZnC_4–ZnN_4, $ZnCN_3$–ZnC_3N and ZnC_2N_2–ZnC_2N_2, respectively.

	LDA–CA-PZ			GGA–PBE			
Model	M4	M13	M22	M4	M13	M22	Exp. [12, 13]
a (Å)	5.7925	5.7968	5.8126	5.9497	5.9547	5.9734	5.9227 5.9328
b (Å)	5.7925	5.7969	5.8126	5.9497	5.9548	5.9735	5.9227 5.9328
c (Å)	5.7925	5.7969	5.7714	5.9497	5.9548	5.9231	5.9227 5.9328
Cell volume ($Å^3$)	194.36	194.79	195.00	210.61	211.15	211.35	207.76 208.82
Energy/unit cell (eV)	−5127.949	−5127.928	−5127.921	−5121.644	−5121.645	−5121.645	
Band gap (eV)	5.63	5.53	5.45	5.78	5.71	5.64	

$Zn(CN)_2$ unit cells calculated by GGA and LDA together with the experimental results are shown in table 1 and table 2, respectively. It is known that LDA and GGA may slightly underestimate and overestimate the lattice parameters or cell volumes.

As shown in table 1, the calculated lattice parameters and equilibrium volumes in optimized unit cells with CdC_4–CdN_4 or CdC_3N–$CdCN_3$ tetrahedra by LDA agree better with experimental values, and the discrepancy is less than 0.65%. The lowest total energy is found for the unit cell with CdC_2N_2–CdC_2N_2 tetrahedra by both LDA and GGA calculations, indicating that Cd bonding to two C and two N atoms is the most favorable among all the possible configurations. However, the difference of total energy among the relaxed unit cells is very small, less than 0.05 eV by LDA and 0.065 eV by GGA. It implies that all MC_xN_{4-x} tetrahedra are quite possibly coexisting with CdC_2N_2–CdC_2N_2 tetrahedra dominating when a $Cd(CN)_2$ sample is prepared. The earlier proposed ordered $Cd(CN)_2$ structure would contain equal amounts of CdC_4 and CdN_4 tetrahedra [18]. However, ^{113}Cd NMR measurements for $Cd(CN)_2$ showed that the sample was dominated by CdC_2N_2 and the existence of CdC_4, $CdCN_3$, CdC_2N_2, CdC_3N and CdN_4 was also revealed [19]. Our total energy calculations not only agree well with the experimental results but also explain why the species coexist with CdC_2N_2 dominating.

As shown in table 2, the lattice parameters of $Zn(CN)_2$ calculated by GGA agree better with the experimental values. The total energies calculated for different unit cells of $Zn(CN)_2$ show an even smaller discrepancy, less than 0.028 eV by LDA and 0.001 eV by GGA. Therefore, it is difficult to predict which tetrahedral combination of ZnC_xN_{4-x} is most preferred. The C–N orientational disorder in $M(CN)_2$ (M = Cd or Zn) structure can be attributed to the very small energy discrepancy in MC_xN_{4-x} tetrahedra. This disorder character of structure was also found in some other compound with single metal centers and cyanide-bridges, such as $Ga(CN)_3$ [33] and AgCN [34], but not in the Prussian blue family [15–17] in which two kinds of metal centers exist in the polyhedra, in which each metal center is surrounded either by carbon or by nitrogen atoms.

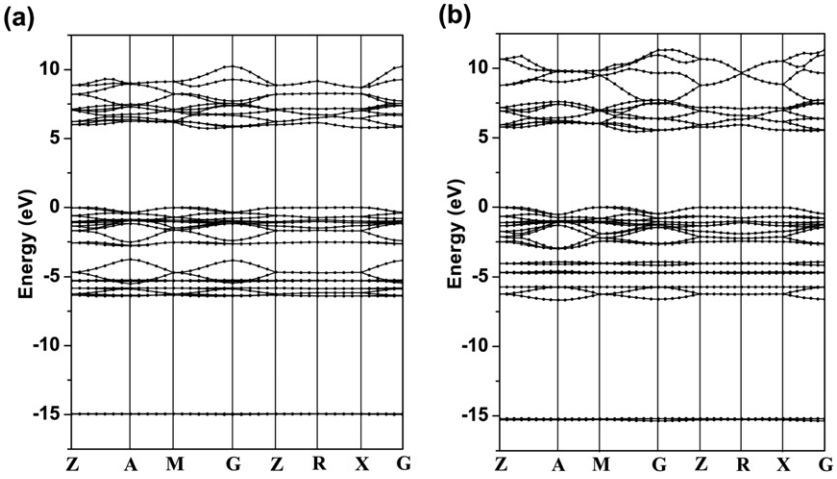

Figure 2. Calculated band structure of (a) $Cd(CN)_2$ and (b) $Zn(CN)_2$ with MC_2N_2–MC_2N_2 tetrahedra by LDA.

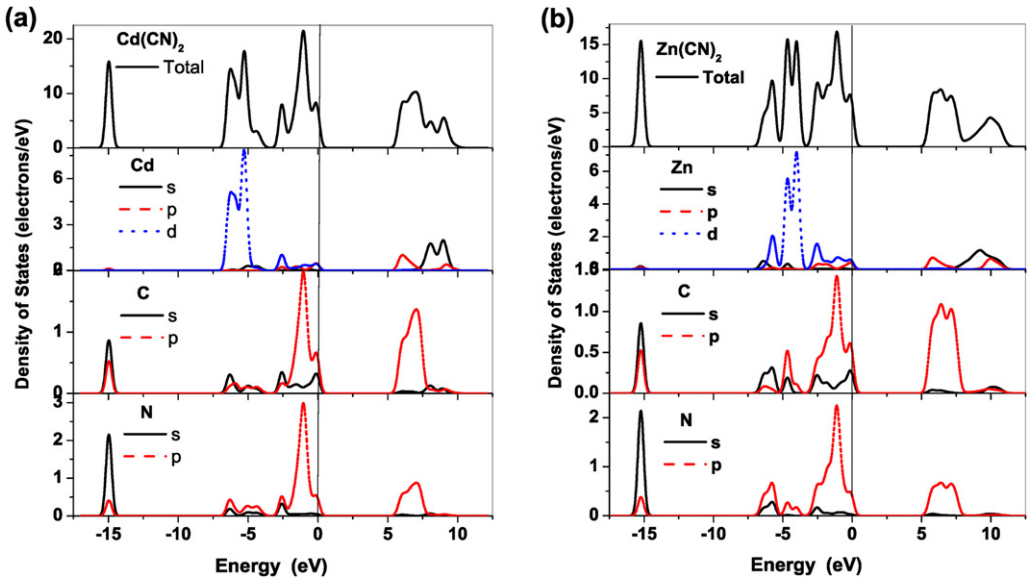

Figure 3. Calculated total DOS and PDOS of (a) $Cd(CN)_2$ and (b) $Zn(CN)_2$ with MC_2N_2–MC_2N_2 tetrahedra by LDA.

3.2. Electronic and bonding characters

3.2.1. Band structure, density of states and partial density of states. The calculated electronic structures by LDA and GGA for the three possible configurations of $Cd(CN)_2$ and $Zn(CN)_2$ are similar and hence we present in figures 2(a) and (b) only the band structures of $Cd(CN)_2$ and $Zn(CN)_2$ with the configuration of cyanide-bridged MC_2N_2 tetrahedra, respectively. The band gap values are listed in tables 1 and 2. Both are indirect band gap insulators with gap widths of over 5.5 eV. This should be considered as the lowest limit since it is well known that both LDA and GGA generally underestimate the band gap of insulators.

Three valence bands appear around −15, −5 eV and between −3 and 0 eV, respectively and a conduction band above 5.5 eV. PDOS and total DOS calculations (figure 3) give an insight into the origins of these bands. The 2s and 2p orbitals of C and N hybridize and contribute to the lowest valence band. The bands around −5 eV and between −3 and 0 eV originate from Cd 4d or Zn 3d, C/N 2s and 2p orbitals. Moreover, C/N 2p orbitals contribute to the lower while Cd 5s and 4p or Zn 4s and 3p orbitals to the higher part of the conduction band. The strong hybridization and highly localized character of the C/N 2s and 2p orbitals around −15 eV suggest that this band corresponds to the C≡N bonds, which are much stronger than the M–C/N bonds originating from the hybridization of the Cd 4d or Zn 3d with the C/N 2s and 2p orbitals between −7 and 0 eV. It should be pointed out that the C≡N bond is stronger in $Zn(CN)_2$ than in $Cd(CN)_2$ and the same happens for the Zn–C/N and Cd–C/N bonds because of the lower energy of the bonds in $Zn(CN)_2$.

3.2.2. Effective charge and bond order. In order to give a quantitative analysis of the bonds, Mulliken effective charges and the bond order (also called the overlap population) values for different unit cells were calculated and are shown in table 3. The effective charges are the total number of calculated

Table 3. Calculated Mulliken population of $Cd(CN)_2$ and $Zn(CN)_2$. 'M4' and 'M22' represent the tetrahedra configuration of MC_4–MN_4 and MC_2N_2–MC_2N_2 (M = Cd or Zn), respectively.

		LDA		GGA		
		Model				
		M4	M22	M4	M22	Exp. [13]
		$Cd(CN)_2$				
Effective charges (electrons)	Cd(1)	10.77	10.93	10.72	10.87	
	Cd(2)	11.09	10.93	11.02	10.87	
	N	5.49	5.47	5.50	5.48	
	C	4.05	4.07	4.07	4.09	
Bond order (bond length (Å))	C–N	1.76 (1.173)	1.77 (1.172)	1.74 (1.181)	1.75 (1.180)	(1.200)
	Cd–N	0.30 (2.132)	0.28 (2.163)	0.28 (2.202)	0.25 (2.241)	(2.138)
	Cd–C	0.43 (2.166)	0.45 (2.142)	0.40 (2.239)	0.42 (2.209)	(2.138)
		$Zn(CN)_2$				
Effective charges (electrons)	Zn(1)	10.74	10.95	10.71	10.9	
	Zn(2)	11.17	10.95	11.09	10.9	
	N	5.48	5.46	5.49	5.47	
	C	4.05	4.06	4.06	4.08	
Bond order (bond length (Å))	C–N	1.82 (1.172)	1.82 (1.172)	1.79 (1.180)	1.79 (1.179)	(1.164)
	Zn–N	0.41 (1.901)	0.39 (1.915)	0.38 (1.965)	0.36 (1.987)	(1.987)
	Zn–C	0.52 (1.943)	0.53 (1.937)	0.49 (2.008)	0.50 (1.995)	(1.987)

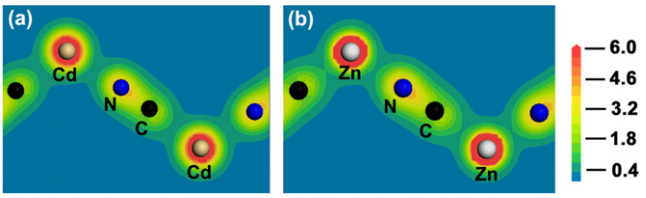

Figure 4. Electronic charge density on a $(01\bar{1})$ plane of (a) $Cd(CN)_2$ and (b) $Zn(CN)_2$ with MC_2N_2–MC_2N_2 tetrahedra.

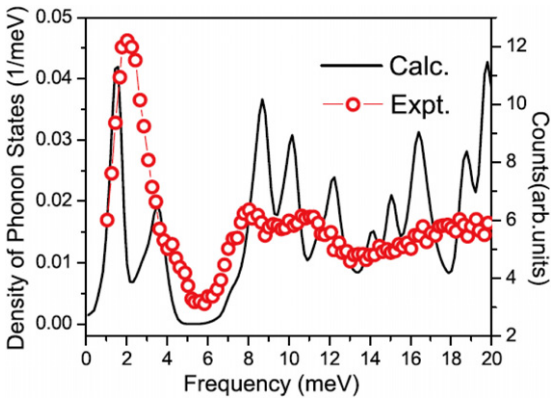

Figure 5. The comparison of the calculated (black line, left vertical axis) and measured [22] (red circles, right vertical axis) phonon density of states in $Zn(CN)_2$.

valence electrons on each atom and provide information on charge transfer. The bond order (BO) is a convenient way to quantify the strength of bonding between a pair of atoms [35]. A value of zero corresponds to an ideal ionic bond while larger values indicate a more covalent nature of the bond [30]. The BO values, depending on the configurations and calculation method, of C≡N are 1.74–1.77 in $Cd(CN)_2$ and 1.79–1.82 in $Zn(CN)_2$, which are much higher than those of Cd–C/N (0.40–0.45/0.25–0.30) and Zn–C/N (0.49–0.53/0.36–0.41), indicating a highly covalent C≡N and the ionic nature of M–C/N bonds. It means that the C≡N bonds are much stronger than the Cd/Zn–C/N bonds. It is found that the C≡N bonds in CdC_2N_2–CdC_2N_2 are slightly stronger than in CdC_4–CdN_4 configurations while they have no difference in ZnC_2N_2–ZnC_2N_2 and ZnC_4–ZnN_4. These are consistent with our minimum energy, band structure and PDOS analysis. In addition, it is also found the M–C bonds are stronger than the M–N bonds. This is further evidenced by the charge transfer from metals to C or N, for example, 0.91 electrons from Cd to C and 1.23 electrons from Cd to N in the unit cell of MC_4–MN_4 by LDA.

In order to reveal the bonding nature of M–C and M–N further, we present in figure 4 the distribution of valence charge densities on the $(01\bar{1})$ plane of $Cd(CN)_2$ and $Zn(CN)_2$ unit cells with MC_2N_2–MC_2N_2 tetrahedra configuration. Strong covalent bonding between C and N atoms is evidenced by the high charge density distribution along the C–N direction. There are spherical-like charge density contours around the metal cations and nonzero charge densities (about 0.4 electrons $Å^{-3}$) in the midpoints between the metals and C/N atoms, confirming the higher ionic bonding nature of M–C/N. The Zn–C/N bonds have a higher covalent degree and are hence slightly stronger than the Cd–C/N bonds because more valence charges are distributed in the mid area between Zn and C/N atoms, which is consistent with the higher overlapping of the electronic states between Zn and C/N atoms indicated by the PDOS of $Zn(CN)_2$.

3.2.3. Elastic properties. The elastic constants and bulk modulus (B_0) of $Cd(CN)_2$ and $Zn(CN)_2$ with fully ordered units (space group $P\bar{4}3m$) were calculated by LDA and GGA and listed in table 4 together with the calculated and

Table 4. Calculated elastic constants, bulk moduli of $Cd(CN)_2$ and $Zn(CN)_2$ with MC_4–MN_4 tetrahedra. The theoretical and experimental values of $Zn(CN)_2$ in [36] are listed for comparison.

		This work				Ref. [36]	
		$Cd(CN)_2$		$Zn(CN)_2$		$Zn(CN)_2$	
Compound		LDA	GGA	LDA	GGA	Calc.	Expt.
Elastic constants	$c11$	43.40	34.83	59.47	48.50		
	$c44$	3.38	5.97	16.18	11.91		
	$c12$	40.97	32.13	54.52	43.23		
Bulk modulus (GP)		41.8	33.03	56.2	45.0	88	25 ± 11
Compressibility		0.024	0.018	0.018	0.022		

Table 5. Calculated phonon frequencies in ordered $Cd(CN)_2$ and $Zn(CN)_2$ with MC_4–MN_4 tetrahedra (i.e. space group $P\bar{4}3m$), their classification, mode assignments and Grüneisen parameters. Among the translational modes of CN ions, '$\perp$' represents the transverse motion away from the $M\cdots M'$ axis, while '$\parallel$' represents the longitudinal motion along the $M\cdots M'$ axis. The theoretical and experimental values of $Zn(CN)_2$ in [36] and [21] are also listed for comparison.

			Calc.						Expt.	
			This work				Ref [36]		Refs [21, 36]	
			$Cd(CN)_2$		$Zn(CN)_2$		$Zn(CN)_2$		$Zn(CN)_2$	
Modes		Symmetry	Freq. (cm^{-1})	γ_1	Freq. (cm^{-1})	γ_1	Freq. (cm^{-1})	γ_1	Freq. (cm^{-1})	γ_1
Cd or Zn lattice		F2	156 (IR, R)	1.37	220 (IR, R)	1.33	388	0.45	216 (R)	−0.50(15)
CN trans.		F1	40	−31.4	51	−22.7	143	−14.3		
	$\perp$	E	124 (R)	−1.07	164 (R)	−0.65	255	−1.5		
		F2	126 (IR, R)	−1.73	174 (IR, R)	−1.1	352	−0.13	178 (IR)	
	$\parallel$	A1	458 (R)	1.91	505 (R)	1.65	564	1.1		
		F2	444 (IR, R)	1.60	509 (IR, R)	1.96	596	1.4	461 (IR)	
CN libr.		F1	228	−2.43	259	−2.52	288	−8.0		
		F2	286 (IR, R)	−1.18	341 (IR, R)	−0.86	326	−7	339 (R)	
		E	290 (R)	−0.94	349 (R)	−0.64	357	−6.2	343 (R)	−0.54(2)
CN int.		F2	2191 (IR, R)	0.22	2207 (IR, R)	0.29	2232	1.5	2218 (IR)	
		A1	2197 (R)	0.22	2216 (R)	0.30	2245	1.5	2221 (R)	0.14(1)

experimental data for $Zn(CN)_2$ in [36]. The elastic constants in table 4 obey the mechanical stability conditions in a cubic crystal, such as $c_{11} - c_{12} > 0$, $c_{11} > 0$, $c_{44} > 0$, $c_{11} + 2c_{12} > 0$ and $c_{12} < B < c_{11}$. $Cd(CN)_2$ with a less rigid framework than $Zn(CN)_2$ has smaller bulk modulus and lower shear modulus. These framework structures are generally quite soft with relatively low shear modulus (c_{44}).

3.3. Vibrational properties

It is not straightforward to incorporate random disorder in ab initio calculations, so the ordered structure of $M(CN)_2$ with MC_4–MN_4 tetrahedra (i.e. space group $P\bar{4}3m$) was used for the calculation and investigation of phonon modes due to its higher symmetry. The calculated zone center optic phonon frequencies and the corresponding identification of each mode as Raman and/or IR active are shown in table 5. The experimental data for $Zn(CN)_2$ in [21, 36] are also listed for comparison. Group theory analysis for $M(CN)_2$ (space group $P\bar{4}3m$) predicts eleven optical modes in which nine are Raman and five are IR active. According to the phonon eigenvectors and group theory analysis [21], these modes can be classified into 5 translational (external), 3 librational (external), 2 internal (stretching) vibrations of the C≡N units and 1 lattice vibration of the metal ions.

In order to investigate the role of different phonons on thermal expansion, the first-principles calculations were performed at different hydrostatic pressures and the phonon frequencies as a function of pressure were obtained. As the pressure is increased to above 0.8 GP for $Cd(CN)_2$ and 1.0 GP for $Zn(CN)_2$, the ω versus P dependence is nonlinear for the lowest-energy phonon modes (i.e. 40 cm^{-1} for $Cd(CN)_2$ and 51 cm^{-1} for $Zn(CN)_2$), and hence not considered in obtaining the Grüneisen parameters γ_i. With the value of B_0 (where B_0 is taken as 45 GP for $Zn(CN)_2$ and 33 GP for $Cd(CN)_2$) calculated by us, the Grüneisen parameters ($\gamma_i = B_0\omega_i^{-1}\partial\omega_i/\partial P$) of the phonon modes were calculated and shown in table 5. It is worth noting that 6 out of the 11 optical modes exhibit negative Grüneisen parameters, which correspond to translational or librational motions of C≡N units.

The linear thermal expansion coefficient α can be written in terms of the Grüneisen parameters as $\alpha = \frac{k}{3VB_0}\sum_i p_i\gamma_i(\frac{\hbar\omega_i}{kT})^2\exp(\hbar\omega_i/kT)[\exp(\hbar\omega_i/kT)-1]^{-2}$, where V is the unit cell volume containing two formula units of $M(CN)_2$, p_i is the degeneracy of the phonon mode with frequency ω_i at the Brillouin zone center. By using the equation, the thermal expansion coefficients at 5 K are calculated to be -21×10^{-6} K^{-1} for $Zn(CN)_2$ and -39×10^{-6} K^{-1} for $Cd(CN)_2$, in agreement with the experimental

values [13]. The discrepancies of γ_i and α between experiment and theory are mainly due to the fact that our model with ordered structure is based on a 0 K model. It does not quantitatively account for dynamical processes and distortion, which must present at higher temperatures and pressures.

The calculated lowest-energy mode in [36] ended at 143 cm^{-1} for $Zn(CN)_2$, which was assigned to the experimentally observed IR active mode at 178 cm^{-1}. However, the lowest-energy optic phonon modes calculated by us are at 51 cm^{-1} for $Zn(CN)_2$ and 40 cm^{-1} for $Cd(CN)_2$, both of which are Raman and IR inactive. As can be seen from tables 4 and 5, the mode frequencies, their Grüneisen parameters and bulk modulus calculated by us are much closer to the experimental values than those reported in [36].

3.4. Negative thermal expansion mechanisms

The phonon modes are directly responsible for thermal expansion in a material. Further investigation on the above phonon's eigenvectors reveals that the translational modes of C≡N units can be subdivided into two subclasses corresponding to the transverse motion away from the $M\cdots M'$ axis and the longitudinal motion along the $M\cdots M'$ axis. The longitudinal modes at 444 and 458 cm^{-1} for $Cd(CN)_2$ and 505 and 509 cm^{-1} for $Zn(CN)_2$ are from the motions along the $M\cdots M'$ axis of the C≡N rigid unit. They have positive Grüneisen parameters and hence do not contribute to the negative thermal expansion. Nevertheless, the transverse translational modes at 40, 124 and 126 cm^{-1} for $Cd(CN)_2$ and at 51, 164 and 174 cm^{-1} for $Zn(CN)_2$ from the motions perpendicular to the $M\cdots M'$ axis of the C≡N rigid unit and the librational modes at 228, 286 and 290 cm^{-1} for $Cd(CN)_2$ and at 259, 341 and 349 cm^{-1} for $Zn(CN)_2$ give rise to negative Grüneisen parameters and therefore contribute to the negative thermal expansion. Transverse vibrations of the C and N atoms in the same (transverse translational modes) or opposite (librational modes) directions have the same effect of drawing the anchoring metal atoms closer. The lowest-energy optic phonon modes at 40 and 51 cm^{-1} possess the largest negative Grüneisen parameters (−31.4 for $Cd(CN)_2$ and −22.7 for $Zn(CN)_2$) and therefore they have the largest contribution among all the optical phonons to the negative thermal expansion for $Cd(CN)_2$ and $Zn(CN)_2$. In addition, the calculated Grüneisen parameters explain also why $Cd(CN)_2$ has a larger NTE coefficient than $Zn(CN)_2$ [13].

In ideal geometries, $M(CN)_2$ topologies contain linearly bridged coordination polyhedra, i.e. M–CN–M in equilibrium is arranged at 180°. As discussed in section 3.2, C≡N bonds are much stiffer than the M–C/N bonds. The weaker M–C/N bonds are expected to decrease the energy of motion of the C/N atoms perpendicular to the M–CN–M axis, favoring strong transverse motion of the cyanide-bridge and resulting in nonlinear M–CN–M geometries and a contraction in non-nearest-neighbor distances. The NTE coefficient of $Zn(CN)_2$ being smaller than that of $Cd(CN)_2$ can be attributed to the correlation between bond strength and vibrational bending flexibility. The Zn–C/N bonds are stronger than the Cd–C/N bonds and therefore more effectively dampen the transverse vibrations of the carbon and nitrogen atoms.

Besides optical phonons, acoustic phonons may also contribute to the NTE effect. Inelastic neutron scattering revealed a lowest-energy peak near 2 meV (∼16 cm^{-1}) which has also a negative Grüneisen parameter [22]. We calculated the phonon density of states in $Zn(CN)_2$ (figure 5) and confirmed the existence of this mode. This mode can not be attributed to a zone center optical phonon mode since the lowest optical mode ends up at 51 cm^{-1} by our calculation. It can be attributed to a transverse acoustic mode from the dispersion curves and has a large contribution to the NTE coefficient of $Zn(CN)_2$ [37].

4. Conclusion

In conclusion, we have carried out a systematic investigation on the geometric and electronic structures, bonding characters, elastic constants and zone center phonon modes of $Cd(CN)_2$ and $Zn(CN)_2$ using the first-principles method. The total energy calculations on different unit cells indicate that their disordered structures originate from the slight energy differences of MC_xN_{4-x} tetrahedra. Both crystals are insulators with indirect band gaps of over 5.5 eV and have a relatively low bulk modulus. Effective charges and band order analyses reveal that the $M(CN)_2$ (M = Cd, Zn) frameworks include much stiffer C≡N and weaker M–C/N bonds, which account for the flexing of the M–CN–M linkage during the transverse motion of the cyanide-bridge. The transverse translational and the librational modes give rise to negative Grüneisen parameters and therefore contribute to the negative thermal expansion. Transverse vibrations of the C and N atoms in the same (transverse translational modes) or opposite (librational modes) directions have the same effect of drawing the anchoring metal atoms closer. Among all the optical phonon modes, the lowest-energy transverse translational modes at 40 or 51 cm^{-1} which are neither Raman nor infrared active in respectively $Cd(CN)_2$ and $Zn(CN)_2$ give rise to the largest contribution to the NTE effect. Besides the mentioned optical phonons, the large contribution from transverse acoustic phonons to NTE mechanisms is obvious.

Acknowledgments

The authors are grateful to Professor Zhenyu Zhang for helpful discussion. This work was supported by the National Natural Science Foundation of China (Grant No. 10574113) and the Natural Science Foundation of the education department of Henan Province of China (Grant No. 2008A140012).

References

[1] Mary T A, Evans J S O, Vogt T and Sleight A W 1996 *Science* **272** 90
[2] Wang K and Reeber R R 2000 *Appl. Phys. Lett.* **76** 2203
[3] Yamamura Y, Nakajima N, Tsuji T, Iwasa Y, Saito K and Sorai M 2002 *Solid State Commun.* **121** 213
[4] Carlson S and Andersen A M K 2001 *J. Appl. Crystallogr.* **34** 7
[5] Evans J S O, Mary T A and Sleight A W 1998 *J. Solid State Chem.* **137** 148

[6] Lightfoot P, Woodcock D A, Maple M J, Villaescusa L A and Wright P A 2001 *J. Mater. Chem.* **11** 212
[7] Attfield M P and Sleight A W 1998 *Chem. Mater.* **10** 2013
[8] Amos T G and Sleight A W 2001 *J. Solid State Chem.* **160** 230
[9] Amos T, Yokochi A and Sleight A W 1998 *J. Solid State Chem.* **141** 303
[10] Sanson A, Rocca F, Dalba G, Fornasini P, Grisenti R, Dapiaggi M and Artioli G 2006 *Phys. Rev.* B **73** 214305
[11] Artioli G, Dapiaggi M, Fornasini P, Sanson A, Rocca F and Merli M 2006 *J. Phys. Chem. Solids* **67** 1918
[12] Williams D J, Partin D E, Lincoln F J, Kouvetakis J and O'Keeffe M 1997 *J. Solid State Chem.* **134** 164
[13] Goodwin A L and Kepert C J 2005 *Phys. Rev.* B **71** 140301(R)
[14] Chapman K W, Chupas P J and Kepert C J 2005 *J. Am. Chem. Soc.* **127** 15630
[15] Margadonna S, Prassides K and Fitch A N 2004 *J. Am. Chem. Soc.* **126** 15390
[16] Goodwin A L, Chapman K W and Kepert C J 2005 *J. Am. Chem. Soc.* **127** 17980
[17] Chapman K W, Chupas P J and Kepert C J 2006 *J. Am. Chem. Soc.* **128** 7009
[18] Hoskins B F and Robson R 1990 *J. Am. Chem. Soc.* **112** 1546
[19] Nishikiori S, Ratcliffe C I and Ripmeester J A 1990 *Can. J. Chem.* **68** 2270
[20] Hahn Th 2005 *International Tables for Crystallography* 5th edn, vol A *Space-Group Symmetry* (Dordrecht: Kluwer) p 683
[21] Ravindran T R, Arora A K and Sairam T N 2007 *J. Raman Spectrosc.* **38** 283
[22] Chapman K W, Hagen M, Kepert C J and Manuel P 2006 *Physica* B **385/386** 60
[23] Payne M C, Teter M P, Allan D C, Arias T A and Joannopoulos J D 1992 *Rev. Mod. Phys.* **64** 1045
[24] Segall M, Lindan P, Probert M, Pickard C, Hasnip P, Clark S and Payne M 2002 *J. Phys.: Condens. Matter* **14** 2717
[25] Perdew J P, Burke K and Ernzerhof M 1996 *Phys. Rev. Lett.* **77** 3865
[26] Perdew J P and Zunger A 1981 *Phys. Rev.* B **23** 5048
[27] Vanderbilt D 1990 *Phys. Rev.* B **41** 7892
[28] Monkhorst H J and Pack J D 1976 *Phys. Rev.* B **13** 5188
[29] Pfrommer B G, Cote M, Louie S G and Cohen M L 1997 *J. Comput. Phys.* **131** 133
[30] Segall M D, Shah R, Pickard C J and Payne M C 1996 *Phys. Rev.* B **54** 16317
[31] Lee M H 1996 *PhD Thesis* Cambridge University
[32] Baroni S, Gironcoli S, Corso A and Giannozzi P 2001 *Rev. Mod. Phys.* **73** 515
[33] Brousseau L C, Williams D, Kouvetakis J and O'Keeffe M 1997 *J. Am. Chem. Soc.* **119** 6292
[34] Bryce D L and Wasylishen R E 2002 *Inorg. Chem.* **41** 4131
[35] Ching W Y and Xu Y 1999 *Phys. Rev.* B **59** 12815
[36] Ravindran T R, Arora A K, Chandra S, Valsakumar M C and Shekar N V C 2007 *Phys. Rev.* B **76** 054302
[37] Zwanziger J W 2007 *Phys. Rev.* B **76** 052102